Biosensors and Bioelectronics 143 (2019) 111600

Contents lists available at ScienceDirect

Biosensors and Bioelectronics

journal homepage: www.elsevier.com/locate/bios

CMOS based whole cell impedance sensing: Challenges and future outlook

Ava Hedayatipour*, Shaghayegh Aslanzadeh, Nicole McFarlane

Department of Electrical Engineering and Computer Science, University of Tennessee, Knoxville, TN, USA

ARTICLE INFO

Keywords:
Impedance sensing
Electrical cell-substrate impedance sensing
Electrical impedance spectroscopy
Biological cells
Cell based sensing
CMOS sensor

ABSTRACT

With the increasing need for multi-analyte point-of-care diagnosis devices, cell impedance measurement is a promising technique for integration with other sensing modalities. In this comprehensive review, the theory underlying cell impedance sensing, including the history, complementary metal–oxide–semiconductor (CMOS) based implementations, and applications are critically assessed. Whole cell impedance sensing, also known as electric cell-substrate impedance sensing (ECIS) or electrical impedance spectroscopy (EIS), is an approach for studying and diagnosing living cells in *in-vitro* and *in-vivo* environments. The technique is popular since it is label-free, non-invasive, and low cost when compared to standard biochemical assays. CMOS cell impedance measurement systems have been focused on expanding their applications to numerous aspects of biological, environmental, and food safety applications. This paper presents and evaluates circuit topologies for whole cell impedance measurement. The presented review compares several existing CMOS designs, including the classification, measurement speed, and sensitivity of varying topologies.

1. Introduction

Biochemical assays are the most common method to observe cellular variations. However, many of these assays result in cell death and can only be performed at the end of the experiment. Impedance spectroscopy of whole cells does not require a label or tag and is capable of monitoring cells' behavior in real time. It is also known as electrical impedance spectroscopy, electrical cell-substrate impedance spectroscopy, or electrochemical impedance spectroscopy (Giaever and Keese, 2012; Gu and McFarlane, 2012; Xu et al., 2016; Yu et al., 2015). However, electrochemical impedance spectroscopy implies the presence of a chemical reaction using a three electrode system that is vital to the measurement. On the other hand, the focus of this paper is on whole cell impedance measurements which are performed using only two electrodes. The real-time impedance measurement of single cells, or multiple populations, of cells can increase the useful information extracted from an experiment. The ability to monitor a single cell is dependent on the size of the electrode. Fig. 1. (a) shows the principle of impedance spectroscopy, based on Ohm's law, and a typical cell model (Fig. 1. (b)). A voltage source generates an electric field between two electrodes. The presence, absence, and physical location of cells (or any particle) between these two electrodes modulates the measured electric field. This results in a change of the measured current (Giaever and Keese, 1986). Alternatively, a current source can be applied and the voltage measured. The two electrodes of the system are known as the working electrode, WE, and counter electrode, CE.

Early cell impedance spectroscopy experiments used only standard benchtop laboratory instruments. A time-invariant (DC) voltage was applied to cells adhered to two planar electrodes (Ehret et al., 1998; Giaever and Keese, 1986). The electrodes used in initial studies were large and not made from good conductors resulting in high surface resistance. Thus, the cell resistance was insignificant compared to the electrode. Using AC signals alleviated the high currents and ionization caused by DC signals. A significant resistance, 1 MΩ in Giaever and Keese, limited the current (less than 1 μA) applied at the electrodes. Applied BioPhysics trademarked this technique of real-time cell monitoring using impedance measurements as electric cell-substrate impedance sensing or ECIS (Giaever and Keese, 1986).

All initial cell impedance sensing systems used benchtop instrumentation. A benchtop LCR meter with series resistance was verified that cell impedance increased with and was proportional to changes in concentration, growth, and physiological state (Ehret et al., 1998). A benchtop lock-in amplifier demonstrated cells response to prostaglandin immediately but had a 2-hour delayed response to leukoregulin (Reddy et al. (1998)). As ECIS technology advanced, commercial products have been developed by Applied BioPhysics, Micronit, NuVant, and ACEA Biosciences Inc. (Applied BioPhysics Inc; Applied BioPhysics Inc) (Micronit Microtechnologies Inc) (ACEA Biosciences Inc; NuVant Systems Inc).

The benchtop instruments are connected to single or multiwall

* Corresponding author. Department of Electrical Engineering and Computer Science, 520 Middle Dr, Knoxville, TN, 37996, USA
E-mail address: ahedaya1@vols.utk.edu (A. Hedayatipour).

https://doi.org/10.1016/j.bios.2019.111600
Received 4 June 2019; Received in revised form 5 August 2019; Accepted 13 August 2019
Available online 23 August 2019
0956-5663/

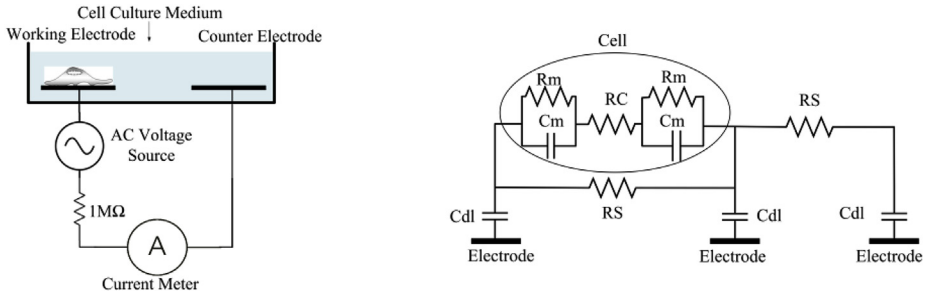

Fig. 1. An overview of impedance sensing. a) Showing the measurement system with the cell on electrode. b) Cell model in media. Rc: intercellular resistance, Cm: membrane capacitance, Rm: membrane resistance, Rs: media resistance, and Cdl: double layer capacitance (Giaever and Keese, 1986).

culture vessels which contain 2-dimensional planar conductive electrodes. However, a reduction in instrumentation size and the promise of high throughput has motivated researchers to harness the low cost and small size of integrated circuits for portable applications such as medical diagnosis and environmental monitoring (Wiest et al., 2006). The successful implementation of a portable system requires the miniaturization while maintaining a high level of robustness and accuracy. This size reduction can be achieved by carefully studying the design of the fluidics, readout electronics and implementing circuit efficiencies. While portability and size reduction through integration is desirable for reducing susceptibility to noise and interference, imperfections due to reliability and fabrication defects may increase in the electronics.

Monitoring the spreading of cells can be a quantitative measure of cell interaction with various macro and nanoparticles or substrates. It can aid the understanding of organ function and influence advancing tissue and organ printing technology. It can be beneficial for studying neuronal networks to enable understanding of the mechanisms underlying how the brain operates.

Some cell-based biosensors use integrated CMOS based technology to measure the biochemical changes of living tissue and convert them into electrical signals (Corcoran and Rechnitz, 1985; Edmondson et al., 2014; Racek, 1995). The advantage of CMOS is minimal power consumption with the possibility of simultaneous temperature control and miniaturization. Using smaller systems (Luo et al., 2016; Park et al., 2019) such as those that use Arduinos to provide a sinusoidal excitation signal and ADCs to read the data can lead to lower power consumption, smaller dimensions, and improved matching of components and temperature coefficients due to bulk batch production. There have been a few review papers on biological sensing (Adiguzel and Kulah, 2012; Lei et al., 2016; Li et al., 2017). Lei et al. investigated the transduction mechanisms of CMOS devices for electrical, magnetic, optical, mechanical, and nuclear spin. Adiguzel et al. focused on capacitive CMOS sensors and CMOS image sensors for applications such as cell viability, cell counting, and DNA sensing. Li et al. presented a review paper for the adaptation of CMOS based electrochemical measurements into integrated microsystems. In contrast, this review paper focuses on whole cell impedance sensing, its applications, limitations, and classification of the circuit topologies.

We present an overview of the development of cell impedance measurements and the paper is organized as follows. The physics, theory, and models underlying cell impedance measurement is discussed in section 2. Applications of cell impedance spectroscopy measurements are discussed in section 3 and section 4 gives a brief overview of system packaging. CMOS based topologies for cell impedance measurement are presented and compared in section 5. Finally, the future outlook and challenges for these technologies are illustrated in section 6.

2. Theory

2.1. Physics and models of cell impedance

Impedance sensors rely on the application of Ohm's law, where either a voltage is applied and current measured, or a current is applied and voltage measured. The impedance of the cell substrate system, V/I, is assumed to be complex and is quantified as a function of frequency. A simple model of a cell in media with three electrodes is depicted in Fig. 1. (b). The impedance seen between the two left electrodes due to the presence of the cell includes the intercellular resistance, Rc, membrane capacitance, Rm, membrane resistance, Cm, media resistance, Rs, and double layer capacitance, Cdl. The impedance seen by the two right electrodes is simply a double layer capacitance and the impedance of the media.

2.2. Mathematical model of a single cell

A cell, consisting of a cell membrane and cytoplasm with the nucleus, may be described using multiple models. Many models rely on Maxwell's mixture theory (Bordi et al., 2002; Foster et al., 1992; Holmes et al., 2009; Koledintseva et al., 2006; Krishna and Paschek, 2000;

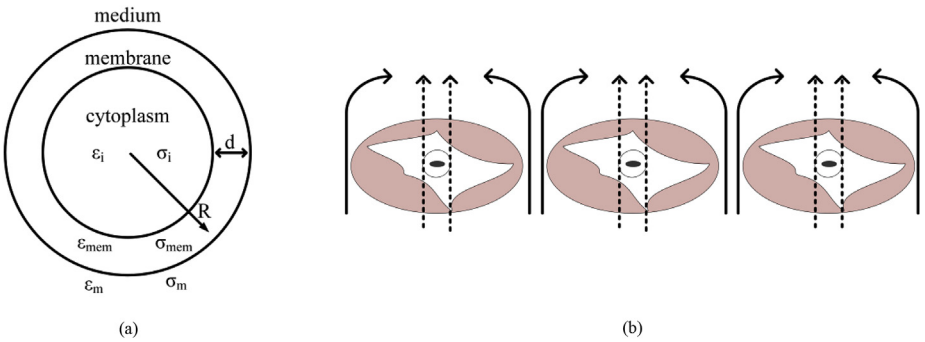

Fig. 2. a) Simplified cell model, showing parameters affecting the impedance of the major parts of the cell (cytoplasm, cell membrane, and growth medium) (Xu et al., 2016). b) Illustration of the current flow passing from the electrodes (solid arrows shows a current path at low frequency, dashed arrows indicate a current path at high frequency) (Giaever and Keese, 1986).

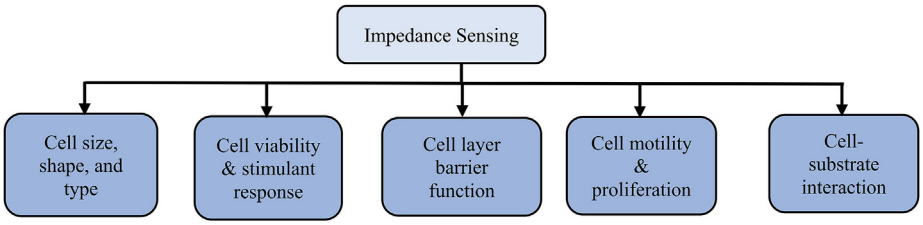

Fig. 3. Cell characteristics measured using impedance sensing. Impedance sensing, discriminates based on uniqueness of cell type, ease of foreign particles crossing the cell membrane, movement of the cells, and cell differentiation and cell growth.

Morgan et al., 2006; Pavlin and Miklavčič, 2003; Sun et al., 2006; Sun and Morgan, 2010). Fig. 2. (a) illustrates the mathematical model based on Maxwell theory. The equivalent complex permittivity of the cell and media, ε_{mix}, is dependent on the complex Clausius-Mossotti, f_{CM}, and permittivity of the suspending medium, ε_m.The fractional volume is the cell area divided by the detection area (Xu et al., 2016),

$$\varepsilon_{mix} = \varepsilon_m \frac{1 + 2\varphi f_{CM}}{1 - \varphi f_{CM}} \tag{1}$$

The complex Clausius-Mossotti factor is (Xu et al., 2016),

$$f_{CM} = \frac{\varepsilon_c - \varepsilon_m}{\varepsilon_c + 2\varepsilon_m} \tag{2}$$

where ε_c, is the permittivity of the cell (Xu et al., 2016),

$$\varepsilon_c = \varepsilon_{mem} \frac{\rho^3 + 2\left(\frac{\varepsilon_i - \varepsilon_m}{\varepsilon_i + 2\varepsilon_m}\right)}{\rho^3 - \left(\frac{\varepsilon_i - \varepsilon_m}{\varepsilon_i + 2\varepsilon_m}\right)} \tag{3}$$

where $\rho = {}^{R}/_{R-d'}$ and R and d' are the radius of the cell and the thickness of the membrane (Xu et al., 2016). ε_m, ε_{mem}, and ε_i represent the permittivity of the medium, cell membrane, and cytoplasm. σ_m, σ_{mem} and σ_i represent the conductivity of the medium, cell membrane, and cytoplasm. This model is simple enough to be adapted to multiple applications, and at the same time takes many parameters into account.

Models, along with a combination of mathematical equations, have been used to diagnose the behavior of fibroblastic cells represented using the equivalent resistance and capacitance (Xiao and Luong, 2003). Others have furthered these models to evaluate the relationship between cells and between the cells and substrate (Goda et al., 2004). Cells adhered on electrodes can be considered as a single passive element or combination of passive elements. These elements are capacitor, resistor-capacitor network, or a constant phase element (CPE). Different frequencies illuminate different cell characteristics such as the shape of the cell, the amount of free space to another cell, and the state of the membrane. There are two current paths in cell impedance experiments (Fig. 2. (b)). The solid arrows show the current path at low frequencies, while the dashed lines show the current path at high frequencies. At relatively low frequencies (up to a few kHz), the AC current applied mostly passes through between adjacent cells, giving data about how close the cells are together and whether they have adhered to the electrode or not (Wegener et al., 2000).

At low frequencies, the cell can be modeled as a small capacitor due to the cell membrane's insulating properties. Under these conditions, the surrounding ionic membrane becomes polarized. The oppositely charged ions in the cell migrate to the two sides of the cell membrane, resulting in an electric dipole (Dandin et al., 2009). At higher frequencies (more than few tens of kHz) more current is capacitively coupled directly through the insulating cell membranes. Therefore at higher frequencies the shape of the cell and cell spreading dominates the impedance. The measured impedance changes as cells attach and grow. They adhere to the electrodes and flatten out, causing an increase in the circuit impedance.

Additionally, the formation of tight junctions between cells at the electrodes has the effect of blocking the electrical current. Cells act as insulators when they attach to a surface and spread since their plasma membrane is in contact with the free space above the electrode. Mammalian cells have been widely used due to their excellent stationery and dynamic interactions with the substrate (Giaever and Keese, 1991, 1993; Wegener et al., 1998, 2000). When cells are at the edge of being non-viable, the membrane is rounded, disrupting the cell-to-cell junction. Non-viable cells may detach from the cell culture surface, allowing greater electrical current to pass. This detachment shows as a decrease in impedance (Bondu et al., 2015). These impedance measurements allow for a depth of information on the real-time biochemical processes beyond the limits of light microscopy, (Yang et al., 2011). Using light scattering and fluorescent labeling can be expensive and time consuming. The need for cheaper, real-time methods makes the development of impedance-based label-free methods a major step forward. In many systems, cells are cultured on gold or other biocompatible conductive electrodes of different sizes and patterns (Albrecht-Buehler, 1977; Giaever and Keese, 1984, 1986, 2012).

3. Applications of whole cell impedance spectroscopy

Impedance spectroscopy has a wide range of applications. The experiments using impedance spectroscopy quantify characteristics that can be expanded from basic cell biology research. Characteristics include cell morphology, cell sorting, cell layer barrier function, cell motility, and cell-substrate interactions and motility. These measurements can be applied in many areas including cancer research, drug screening, environmental pollution, food safety detection, electroporation, pathology, and brain-machine interference study. Fig. 3 lists the characteristic measurements of impedance spectroscopy. Table 1 gives the various applications informed by the measured characteristic. Impedance measurements may be quantified for single cells (Holmes et al., 2009; Liao et al., 2005; Nguyen et al., 2013; Wang et al., 2011),

Table 1
Impedance spectroscopy applications.

Application	Field	Description
Drug and Diagnostic Advancement	Cancer research	Quantitative and qualitative identification of cancerous cells and non-cancerous cells
	Drug screening	Quantifies the dose and resistance to drugs
	Pathology	Laboratory examination tissue for diagnostic or forensic purposes and causes and effects of diseases in medicine.
	Electroporation	Makes the cell membrane more permeable to chemicals, drugs, and DNA.
Safety	Environmental pollution	Quantifying the effect of nanoparticles and non-essential gasses on lung epithelial cells
	Food safety detection	Quantifying the existence of bacteria or other unwanted characteristics
Brain-machine interfaces	Monitoring neuronal cells' activity	Measuring cells' activity lead to more advanced brain machine interfaces.

multiple cells (Edmondson et al., 2014; Giaever and Keese, 1984, 1986; Keese et al., 2004), cells in suspension (Caselli et al., 2010; Davey and Kell, 1996; Evander et al., 2013), cells adhered to the substrates (Luong et al., 2001; Mucha, 2012; Reitinger et al., 2012; Xiao and Luong, 2003) and long-term monitoring (Bagnaninchi and Drummond, 2011; Sengupta et al., 2005; Wegener et al., 2000).

3.1. Adherent application

One of the primary applications of impedance measurement studies viral growth and cellular responses to infectious viral agents, such as respiratory syncytial virus (RSV), alpha herpesviruses (AH), sin nombre virus (SNV), and influenza A virus (IAV) (Bondu et al., 2015; Kilani et al., 2004; McCoy and Wang, 2005). In McCoy and Wang, ECIS, they used to measure real-time monitoring of infection via influenza A. This virus would cause cytopathic effect (CPE) on the cell culture that is difficult to quantify using conventional methods. CPE is exemplified by structural changes in cells that are caused by the infecting virus. Influenza A compromises the cell's viability which results in the cell physically changing shape (e.g. it may ball up instead of being a defined shape) or detaching, resulting in an impedance change (McCoy and Wang, 2005). Effects such as age, presence of bacteria and fungus, and the number of freeze-thaw cycles in perishable and consumable animal protein can be detected by changes in cell morphology and thus detected by whole cell impedance (Zhao et al., 2017).

Dynamic measurements of total electrical resistance across the primary human bronchial epithelial cells (HBEpC) monolayer showed a few kΩ steady-state resistance on wells and infection by alpha-herpes viruses (Pennington and Van de Walle, 2017). A potential key to new genetics based discoveries is quantifying cells as they fall towards the culture surface and adhere to the surface through biochemical processes. Using this culture surface would be useful because they act as an electrolyte and in that case, a constant current source makes a small current AC resulting in a small impedance (Cho and Thielecke, 2008; Luong et al., 2001).

Understanding the cell attachment parameters for anatomical implants is vital in the development and modification of biomaterials. This is because the cell–semiconductor interfaces enable cells to communicate with biological neurons (Parak et al., 1999; Vogler, 1988). These *in-vitro* studies foster an improved understanding cells interaction with the culture surface or substrate. They give information on cells growth, adherence to the surface, and causes of cell change or death. This can advance understanding of tumors, tissue repair, or cell movement (Lauffenburger and Horwitz, 1996). Other recent studies used stem cells to study or treat diseases. Stem cell studies offer insight into cell differentiation and can be used for screening and tracking quality control (Cho et al., 2009; Hildebrandt et al., 2010; Nordberg et al., 2017). A classic approach, still used today, is recording brain cell populations in culture over time. Advancement in cell characteristic measurement using impedance sensing increases the understanding of brain-machine interfaces (Mussa-Ivaldi and Miller, 2003; Nicolelis, 2003). For example it may be used to monitor electrophysiological recordings from distinct mouse brain regions (Fu, T.-M. et al., 2017).

Impedance spectroscopy quantifies the size of a cell which can affect real-time processes. The extracellular matrix (ECM) influences the biophysical surface structure and affects cell-cell interactions, which in turn affects cell survival, differentiation, and proliferation (Itano et al., 2003). Cancer cell attachment and drug induced cellular event monitoring can aid drug discovery, ease patient testing, and lower cost. It can also quantify triggering signals that affect the ECM such as differentiation, cell migration, cell life cycle, and exploring new drugs (Anh-Nguyen et al., 2016; Mamouni and Yang, 2011; Solly et al., 2004; Tran et al., 2016). (Anh-Nguyen et al., 2016).

Proteins, such as plasma fibronectin, gelatin bovine fetuin, or bovine serum albumin, interaction with cells can affect motility and spreading on different substrates. These proteins can be essential for healthy cell behavior (Giaever and Keese, 1986). Cell impedance has been measured using a vacuum pump and dielectrophoresis (DEP) for precise manipulation and positioning. This identified and counted a specific type of cell within a mixture of different cells (Mohanty et al., 2003; Watkins et al., 2011).

As fabrication technology and analog design advances, it enables more sensing circuits to be placed in a single chip. Newly developed multi-parameter cell sensors combine acquisition of different parameters of the cell layer at the location of transducers. These parameters can be cell coverage for monitoring wound healing parameters along with bioluminescence or electrochemical measurements. This makes the measurement more specific and enable studies aimed at reducing scaring and other diseases (Cui et al., 2017; Giaever and Keese, 1984; McGuinness, 2007; Mucha, 2012).

Being label free, impedance spectroscopy is a valuable method for evaluating a large number of cells. It can perform adherent impedance measurement in the cell trapping method. In this method, a fluid flow drives cells between two stick-like metallic electrodes and cells settle on the planar electrodes by gravity and attach to the electrode via biophysical and chemical processes (Narayanamurthy et al., 2017). Cell discrimination is useful for early diagnosis of diseases. To make an early diagnosis, the affected cells must be identified relatively early. Thus, if cells at different stages have different impedance, this is a potentially fast and easy method for early diagnosis. Fig. 4 (a) shows the flow of control fluid, which produces a negative pressure to trap the cell into an analysis cavity where two electrodes were embedded (Han et al., 2007). Single-cell analysis provides a unique understanding of diverse behaviors of cells. Levsky showed that even synchronized culture conditions resulted in a heterogeneous population of expression profiles that can make statistical modeling of cells complex (Levsky and Singer, 2003). For example, in the first steps of the transcriptional program, there is no pathway for every step for each cell. But as it goes, in a variable population of cells, the averaged response of a cell population can dominate the measurement, making single-cell approaches a more robust

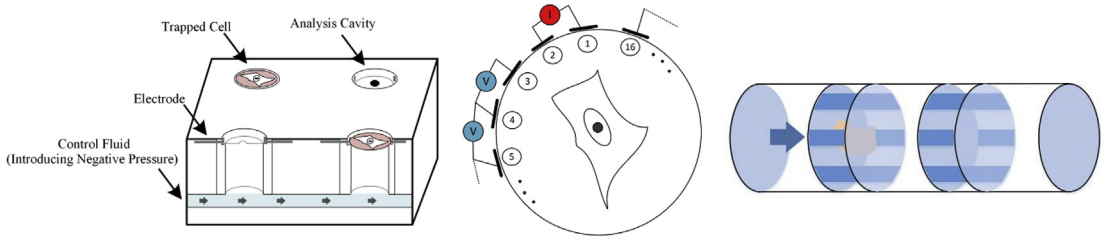

Fig. 4. Cell measurement methods for adherent and non-adherent application. a) Principle of cell trapping for cell discrimination (Han et al., 2007). b) Principle of single cell imaging in a circular 16-electrode chip (Sun et al., 2009). c) Microfluidic impedance-based cytometer (Caselli et al., 2010).

method (Levsky and Singer, 2003). For measurement of adherent cells, there is an unstated assumption that the presence of the cells does not alter the inherent impedance of the electrode or the electrolyte interface. This is validated by the extremely small, nanometer range, electrolyte filled gap under the cell (Mucha, 2012).

3.2. Non-adherent application

For non-adherent cells, microfluidic impedance based cell cytometry can count, identify, and sort cells (Davey and Kell, 1996; Fu, Y. et al., 2017), recent advancements has led to a portable low cost health monitoring system that pair up wirelessly with a smartphone and can run blood samples (Talukder et al., 2017). These type of systems can be made to be wireless. In Sun et al., multiple arrays are fabricated in a circular form around the cell. By injecting current to each pair of electrodes and measuring voltage from other pairs, conductivity distribution map can be obtained. Assuming the electrodes are fabricated in a 16 electrode scheme (Fig. 4 (b)), current is applied through the first two electrodes and the voltage across each pair of electrode measured. 13 sets of current and voltage data is generated. The voltage in the electrode adjacent to injecting ones cannot be measured. The current injection was repeated for 15 sets of electrodes leading to 208 sets to construct the cell. This design implemented by discrete fabrication of the electrodes, switches, multiplexers, and other electronic components caused a significant amount of noise. Another source of error was due to the software enabled data reconstruction (Sun et al., 2009). The same method was used to measure the electrical impedance to reconstruct a 3-dimensional representation. The impedance was measured at various vertical and horizontal positions, and a 3-D image constructed using a mathematical algorithm. The experiment was verified for human breast cancer cells shaped as a spheroid and a triangular pellet (Yang et al., 2017).

Complex samples were analyzed by optically encoding μm-sized polymer particles to create suspension microarrays (Caselli et al., 2010; Davey and Kell, 1996; Nolan and Sklar, 2002). Syringes or micro-pumps drive cells through coplanar electrodes. In Caselli et al. multiple electrode arrays shown in Fig. 4 (c) were used for cell cytometry. Using two arrays instead of 2 coplanar or parallel facing electrode leads to an increase in sensitivity. The sensitivity in reconstructing conductivity distribution, based on electrodes voltage and current data, is the primary concern in EIT (electrical impedance tomography) instruments. In two electrode systems, the measurement is done through the same electrodes that stimulate the system, causing a disturbance. Differential measurements attenuate the disturbance due to electrode impedance (Caselli et al., 2010). In a similar investigation, four electrodes were used where for each measurement instance the AC voltage was supplied to two electrodes along the diagonal line and the current was measured from the remaining electrodes (Caselli et al., 2018).

Cell cytometry analyzes many cells over a short span of time (Wegener et al., 2000; Xiao and Luong, 2003). In continuous flow systems, single cells are monitored for extended periods. Microfluidic devices are very suitable for this application, hydrodynamic cell trapping arrays within a microfluidic device can capture large numbers of individual cells for evaluating different conditions in companion animals such as orthopedic diseases. Since a massive quantity of cells can be processed in a small amount of time, it is amenable to applications requiring high throughput processing. This method is analogous to the classic method of counting the cells colonies of thousands under the microscope (Sun and Morgan, 2010) (Esfandyarpour et al., 2017).

Overall, whether used in adherent or non-adherent applications, many methods exhibit errors and inaccuracies. In adherent methods, the membrane capacitance and size of the cell drifts depending on the length of time they remain on the surface (Xavier et al., 2017). In non-adherent applications, a significant source of measurement inaccuracy is particle position (De Ninno et al., 2017). These variabilities limit the resolution of microfluidic devices. A heterogeneous electric field causes different impedance signals, since the particles travel in different trajectories. To make the particles move in the same trajectory, a non-adherent application was proposed in order to reduce measurement error (Errico et al., 2017).

3.3. Impedance of cells: quantitative measurement examples

In this section, representative quantitative results for cell impedance measurement in cancer research and wound healing are presented. Changes in impedance, usually ranging in a few kΩs, have shown the importance of high accuracy designs. Moreover, many of these applications focus on miniaturized, low cost systems. Impedance has been used to quantify cancer cell stages, explore the effect of cigarette toxins and study wound healing among other applications. Cancer cells have different characteristics than healthy cells in reproduction, adhesion, proliferation rate, maturation, and function. Cell impedance, magnitude, and phase, for normal cells and lung metastasis cells at different stages have been widely investigated (Abiri et al., 2015). In the attachment stage (3.5 hours after the initial drop of cells on electrode), cancer and normal cells act the same, with 80 kΩ impedance. In the spreading stage (6 hours after the initial drop of cells on electrode) the degraded membrane of cancer cells improves the current penetration into the cell the impedance decreases to 20 kΩ, while normal cells remained the same. In the proliferation stage (9 hours after the initial drop of cells on electrode), impedance increased from 20 kΩ to 80 kΩ in cancerous cells while normal cells stayed the same. This difference is visible in the proliferation rate since normal cells need more time for spread and membrane extension. Fig. 5 shows the results of cells at four different stages, normal cells, early stage, invasive breast cancer, and metastasized cell lines. Each represents these different stages, and as the cancer stage increases, the impedance of the cells decrease (Han et al., 2007). Measured impedance is increased by two times over that of normal cells, while electrical stimulation shows more cells at the wound edge, thus increasing wound healing (Wang et al., 2008). As the concentration of the cigarette toxicants increases, cells have lower self-recovery ability to continue proliferating. Normal cells impedance increased by ~14%, while the cell growth was 0% for compromised cells (An et al., 2019).

4. System packaging

To make cell impedance measurements, cells must be close enough to the electrodes to significantly affect the generated electric field (Fig. 6 (a)). The simplest way to do this is to encapsulate the bond wires of a packaged chip and place a well to hold the cells (Fig. 6 (a)). The

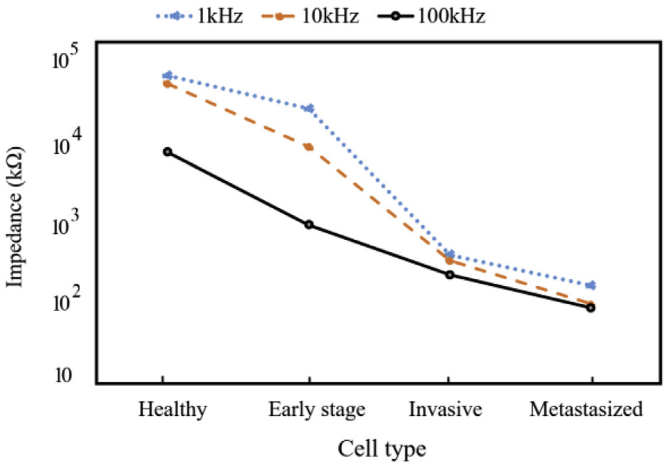

Fig. 5. Impedance of different stages of cancer cells in 3 different frequencies (data extracted from Han et al., 2007).

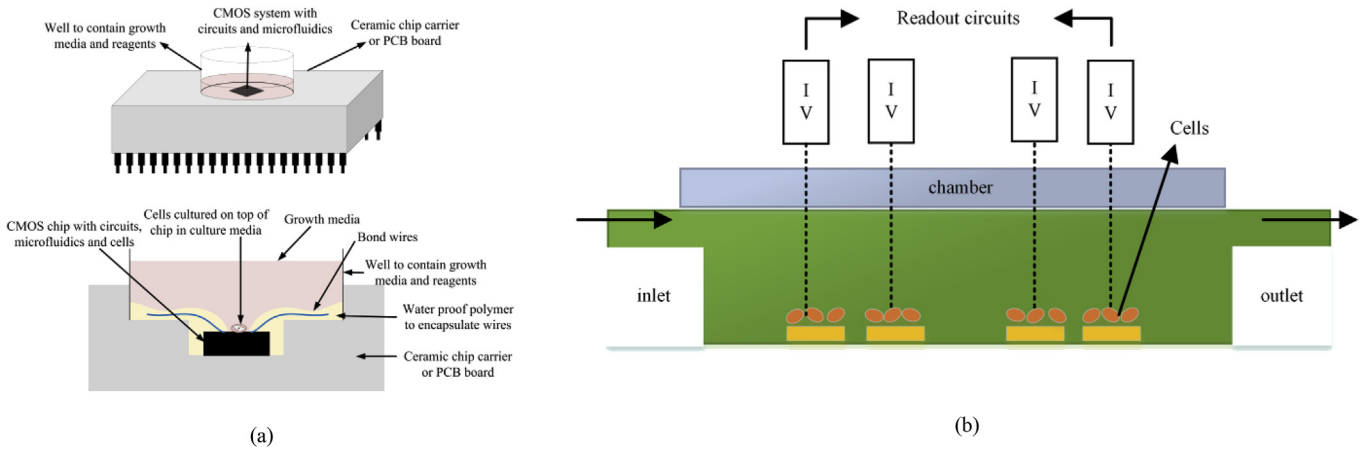

Fig. 6. System packaging overview a) Method of culturing cells onto integrated system. Adapted from (Dandin et al., 2009). b) Microfluidic flow path in DEP/PDMS (Jang and Wang, 2007).

cells are then deposited using standard aseptic methods with a pipette. This method is relatively crude and does not give the user the ability to ensure that the cells are accurately and deterministically placed on the electrodes. Thus, many researchers study methods of conveying the cells using hybrid glass/PDMS/silicon chambers and microenvironments which supports the growth of a confluent syncytium, several cell fusions of a uninuclear cell (Dandin et al., 2009). A microfluidic flow chamber is shown in Fig. 6 (b) (Jang and Wang, 2007).

Using a microfluidic flow chamber, a device was proposed that counts and separates the cells in hematology, oncology, or toxicology. This method measures impedance of individual cells with rates of over 100 samples/s. In this chamber, the differential impedance is measured (Fig. 6 (b)). When a cell passes through the detection area, positive and negative spikes are generated, which can be used for cell counting. When the cell passes through the electrodes, an impedance model can be extracted based on voltage and current gotten from the readout circuit. In this method, alternate switching of reference and measurement electrodes can reveal uneven drift of electrode properties (Gawad et al., 2001).

Other methods of fabrication use the fundamental principles of these steps with minor variations. The medium consists of a fixed volume. It has two channels, one at the input and the other in the output to make the fluid. The electrodes are located at the bottom of the chamber. A type of cell trapping method was proposed in Walker and Beebe in which the limitation of cell resolution for sequential measurement is overcome by integrating a passive pumping method (Walker and Beebe, 2002). In this method, single cells are forced onto the electrodes without using off-chip pumps (Nguyen et al., 2013). Micro-well electrodes and a minimized impedance system (Wang et al., 2011), as well as capture of controlled number of cells in the micro-well arrays have been demonstrated (Shah et al., 2016).

5. Readout electronics topologies

There are many topologies for quantifying cellular impedance. These methods are summarized in Fig. 7. All topologies are based on applying a current (or voltage) and measuring the corresponding voltage (or current). The three topologies rely on impedance to frequency conversion using an implicit analog to digital conversion, swept frequency using a varying sinusoidal frequency source and filtering to return the magnitude and phase through measurement of a time delay, and simultaneous frequencies which potentially decreases the time for measurement. (Kweon et al.), (Won et al., 2016).

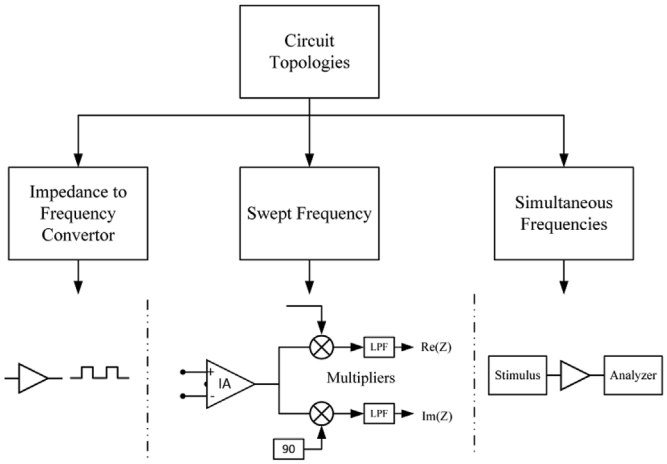

Fig. 7. Topologies used for cell impedance sensing measurements can be divided into three groups.

5.1. Impedance to time or frequency

The measurement principle relies on an making the output frequency proportional to the impedance. A current is periodically sourced and sinked through the impedance. In the first phase, the current charges the impedance and impedance voltage level reaches an amount set by a reference voltage. The reference voltage is in charge of switching the circuit between charge and discharge mode. In the second phase, the voltage decreases because of the current sinking until the voltage gain reaches a minimum set by the reference again.

Fig. 8 shows approaches for impedance to time or frequency conversion. These methods differ in whether they use a known value and the way the output is generated. In one approach, the difference in charge, discharge speed, and voltage drop when injecting current is correlated to the change in impedance (Fig. 8 (a)). In another approach a known value is measured as a base and the change from that value determined (Fig. 8 (b)). The output type can also divide the topologies, where an analog sinusoidal or digital pulse frequency is the output (Fig. 8 (a)). Extra modules may be added to obtain digital data (Fig. 8 (c)). The first method, of course, has the lower power and area but needs additional off-chip processing. However, analog signals can attenuate when transmitted off-chip which may decrease the resolution and accuracy.

Fig. 8 (a) shows an impedance to frequency conversion system (Mucha, 2012). When V_{out} is high, Φ_1 is active, and Φ_2 is low. Therefore, the current, I_0, is injected through the electrode. Extra switches

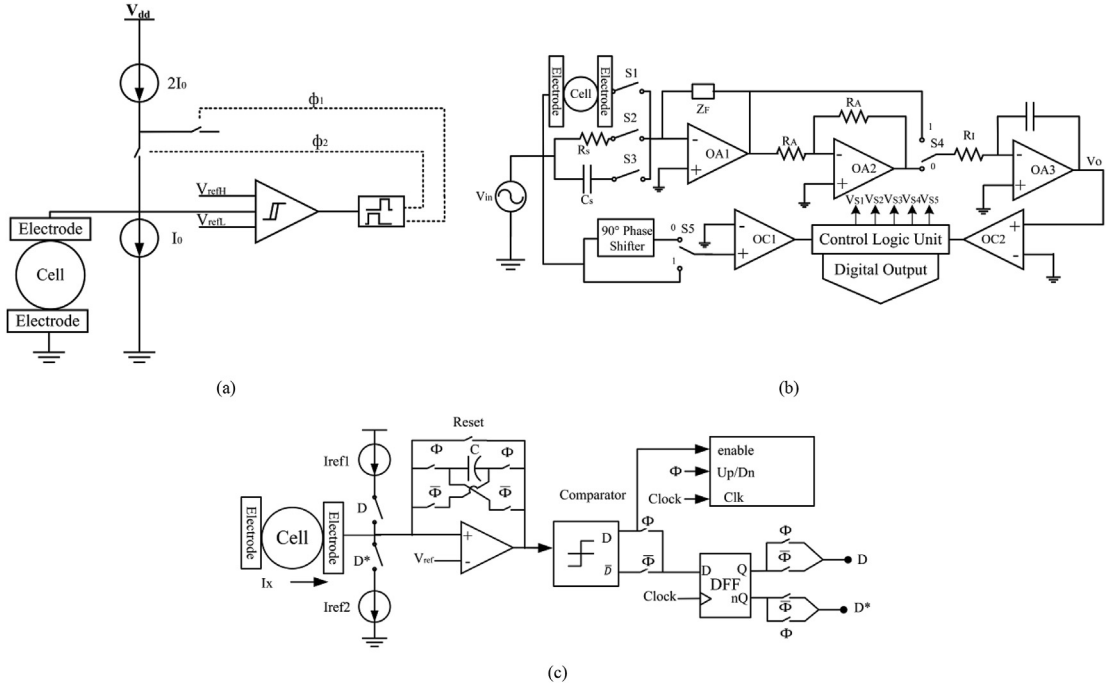

Fig. 8. Illustration of impedance-to-frequency topologies with a) alternate current sink and source leading to a charging and discharging intervals that determine the output frequency (Mucha, 2012), b) using multiple mode for measuring R and C, in each mode first current passing a known value is measured (Rs and Cs) and next the control logic unit change the switches so the unknown values are measured (R and C of cell) (Vooka and George, 2015). c) Impedance-to-digital converter structure that uses the same sink and source method as (a) but adds a digital block and counter to give a digital output as the frequency (Liu et al., 2009).

$$T = 2\frac{C_{el}}{I_0}(\Delta V - 2R_{el}I_0) = 2C_{el}\left(\frac{\Delta V}{I_0} - 2R_{el}\right) \tag{4}$$

such as Φ_2 keeps the channel of the MOSFET active, preventing a short circuit between supply and ground. The charging and discharging intervals determine the output frequency. The electrode potential increases as a switch, Φ_2 closes and the current, I_0, is sourced to it. The potential is continuously compared to V_{refH} as it increases. Once the potential reaches the high voltage reference, $\Phi_2$opens, and I_0 is sinked from the electrode, decreasing the potential, until V_{refL} is reached. The period of a single charge-discharge cycle is,where R_{el} is the resistance and C_{el} the capacitance of the cell. The voltage drop caused by the change of the current through R_{el} from $+I_0$ to $-I_0$ and is related to $\Delta V = V_{refH}$-V_{refL} and $2R_{el}I_0$ (Fig. 8 (a)).

Fig. 8 (b). shows a system where the cell impedance, R_1 and C_1 are compared to R_S and C_S a known resistance and capacitance (Vooka and George, 2015). In this system, only one parameter is measured at a time, mode R or mode C. In the first period, the charging time of a known value is measured. In the second period, the discharging time of the sensing element is measured, and the unknown value of capacitance can be calculated such that,

$$Q_{T2(c)} = 2V_{k2}N_{2c}C_1 \tag{5}$$

where $V_{k2} = C_s\left(\frac{2V_m}{\omega C_1 R_1 C_F}\right)$. N is the number of cycles, C_s is the fixed capacitor, and $V_m = \frac{V_{in}}{2\pi sinft}$.

Fig. 8 (c) shows a high sensitivity impedance to digital frequency converter. It computes and digitizes the real and imaginary part of a signal. The D-flip flop samples the signal through the comparator. φ is a reference square wave while Clk is an external clock for synchronization. The comparator controls the output from the integrator, and the counter digitizes the final result (Liu et al., 2009). A simple phase to digital method using an SR-latch and ring oscillators detects the phase (Hsu et al., 2018). The pulse through the cell was compared to a reference signal generated by an SR-latch. The duty cycle of this phase difference is changed to frequency using a ring oscillator and is stored on a capacitor.

5.2. Swept frequency or lock-in approach

In all the swept frequency approaches, the real and imaginary portion of the signal is extracted by multiplying the signal with the in phase and quadrature signal. These approaches are categorized based on being voltage mode (Fig. 9 (a)) or current mode (Fig. 9 (b)). To increase the accuracy of system, a zero detection block (Fig. 9 (c)) or passive mixers (Fig. 9 (e)) may be used. On-chip implementation of the pytharogator and arctangent modules can eliminate the need for external digital signal processing (Fig. 9 (d)).

In Fig. 9 (a) the DC component proportional to the real and imaginary signals is obtained from the low pass filters (Manickam et al., 2010). The sinusoidal excitation is,

$$I_x = Asin(\omega t + \theta) = \text{asin}(\omega t) + bcos(\omega t) \tag{6}$$

Where I_x is the measured current at the x^{th} electrode, with A and θ being the amplitude and phase of the signal. In this equation, a = $Acos(\theta)$, is the real part of the signal and b = $Asin(\theta)$, is the imaginary part of the signal. By knowing a and b, the impedance information is completely described. The phase and amplitude information of I_x is thus easily obtained. This has been implemented in a number of CMOS implementations where the real and imaginary impedance components are extracted and fully digitized using ADCs, (Yang and Mason, 2008), (Ali et al., 2015). Since the impedance of a cell consists of real and imaginary portions, a stimulation pulse can quantify this complex impedance. A square wave signal stimulates the bio-impedance system,

$$f(t) = \left(\frac{A}{\tau}\right)\left\{u\left(t + \frac{\tau}{2}\right) - u\left(t - \frac{\tau}{2}\right)\right\} \tag{7}$$

where A is the amplitude, τ is the width, and u is the unit step function (Kim et al., 2017). The impedance model is determined from the

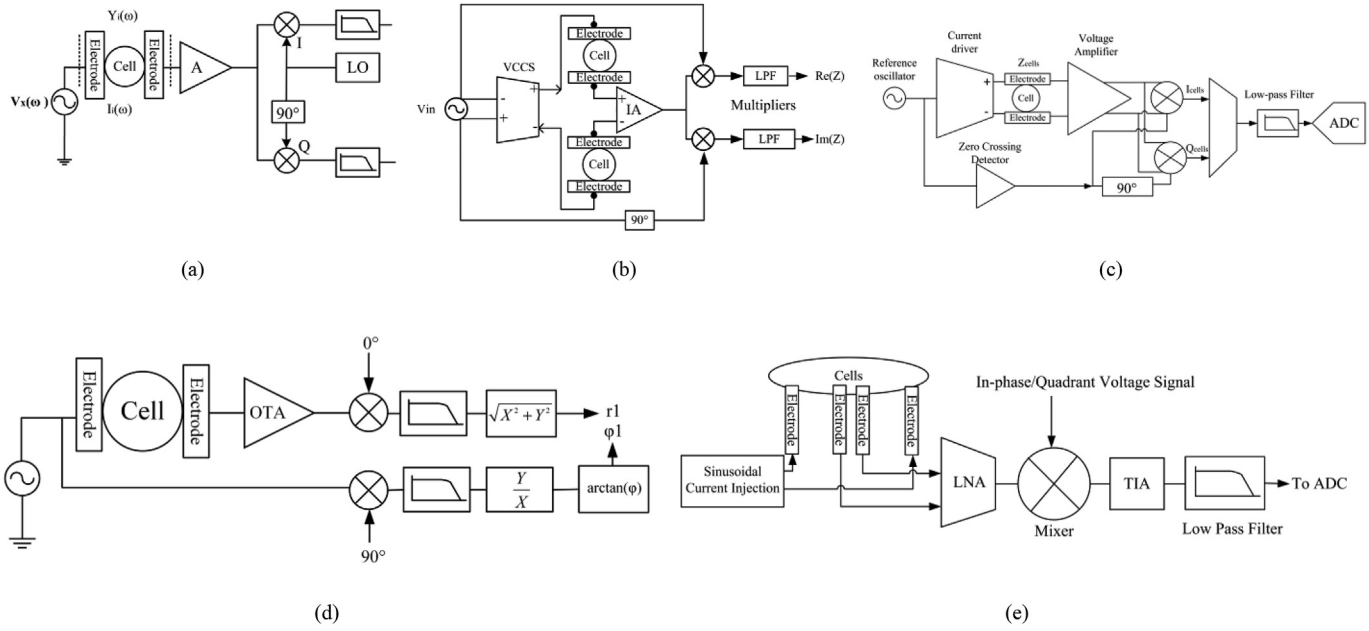

Fig. 9. Different lock-in approaches a) voltage-mode lock-in amplifier sweeps the frequencies of the sinusoidal signal applied to the electrodes and measures the imaginary and real part of the output signal (Manickam et al., 2010). b) current-mode lock-in amplifier with same approach as (a) but supplying current instead of voltage through electrodes (Kassanos et al., 2013). c) zero crossing detector added to impedance detection using lock in amplifier to elimination of high impedance loading (Dungan et al., 2014). d) This approach adds on chip implementation of pythaogator and arctangent to eliminate the need for any external digital signal processing module (Gu and McFarlane, 2015). e) To increase the accuracy of 90° phase difference used in approaches (a) to (d) a passive mixer controlled by digital clock signals is used (Rodriguez et al., 2016).

locations of the zeroes and poles of the transfer function. In the frequency domain we obtain,

$$F(f) = A\frac{\sin(\pi\tau f)}{\pi\tau f} \tag{8}$$

The same method was used to develop a DNA analyzer system. After extracting the imaginary and real components of the signal, digital coefficients were used with an ADC to multiply the biosensor response. The digitized signal accumulates over using a counter, and results in the extraction of the imaginary and real components of the impedance (Jafari et al., 2012). Due to the advantage of summing currents and implementing complex signal processing, such as sum of the squares or division in current mode, a current-mode lock-in amplifier was developed. The advantage of this design is that there is no need for using extra blocks in the digital domain, and the system has a lowered power consumption and area. The design is illustrated in Fig. 9 (b) (Kassanos et al., 2013). Rottigni et al. used the same method of impedance extraction and implemented a handheld bio-impedance system with excellent resolution (Rottigni et al., 2011). An alternative feedback configuration used a rectifier to detect the largest voltage amplitude and an error amplifier with a current oscillator (Yufera and Rueda, 2009). Fig. 9 (c) shows another variation of a lock-in amplifier, where a zero crossing detector and elimination of high impedance loading is performed (Dungan et al., 2014).

In Gu and McFarlane, a new current mode lock-in amplifier was proposed. Many impedance measurement systems use a digital signal processing block to determine the components of the complex impedance obtained from the lock-in's output. Previously, most of the structures are based on voltage mode. The disadvantage of using lock-in amplifiers in voltage mode is that implementing the pythagorator and arctangent in voltage mode is very difficult. To solve this issue, a new current mode lock-in amplifier was proposed. By using this technique, the power consumption and area is kept low due to not requiring external digital signal processing module (Gu and McFarlane, 2015). The system has four channels, each having two sub-channels. These channels determine the components of the impedance (Fig. 9 (d)). This system contains a mixer, low pass filter, trans-conductors, band pass filters and phase shifter (for generating LO signals). The magnitude of the impedance is obtained by the pythogorator, while the divider aids in computing the arctangent. An advantage of this structure is that it includes different cut off frequencies for each channel, so this lock-in amplifier measures the impedance at multiple frequencies simultaneously. Thus, this system is a hybrid of the lock-in approach and the simultaneous frequencies approach. This approach does add to the system size, and there is a tradeoff in the number of electrodes that can be measured with this system in a fixed area.

One of the disadvantages of these systems is that by moving the phase of the system from 90°, the accuracy of the system is compromised. It is somewhat challenging to produce a sinusoidal signal, which is adjustable within a large range (Chen et al., 2017). A battery-less miniaturized implantable device with frequencies from 2 kHz to 2 MHz was developed using a passive mixer controlled by I/Q digital clocks. This method was highly-linear and low power. This method relied on sinusoidal current injection Fig. 9 (e). Using a sinusoidal differential current, the differential voltage drop is measured (Rodriguez et al., 2016). Combining the lock-in approach with mixed signal approaches have also been proposed (Allegri et al., 2018) where the ADC changes the impedance signal and turns it into digital data from which the real and imaginary part of the signal is extracted.

5.3. Simultaneous frequencies or pulsed signal approach

In the swept frequency lock-in approach, the signal must pass through a low pass filter. Thus the measurement time is increased at low frequencies. Additionally, each frequency is applied one at a time. For high frequency resolution systems this will limit the measurement speed. To improve the system measurement time, a multi-frequency signal can be used to stimulate the electrodes. The silicon cochlea creates sinusoidal stimuli at frequencies which are spaced periodically. These stimuli are summed. The “analyzer” part of the cochlea divides the output into the related frequency to establish a relationship between impedance and frequency. The silicon cochlea is effectively an

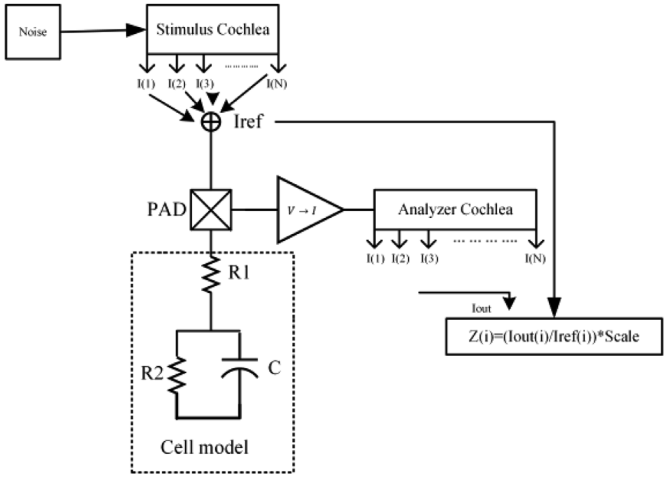

Fig. 10. Cell impedance measurement using silicon cochlea (Hamilton et al., 2009).

excellent filter bank acting as an "analyzer" (Fig. 10). The filters are typically implemented with low power Tau-cells implemented with trans-linear loops (Fig. 11) (Gu, 2016). An implementation of this architecture in a 500 nm and 130 nm process saw mixed results. The implemented filters had relatively wideband width and suffered significantly from effects due to process variations. Thus, the extracted measurement would be very noisy due to the overlap of lower frequencies. The filters should have a much smaller bandwidth to be truly selective frequency filters. The voltage is given by

$$V(s) = Z(s).\ I_{ref} \tag{9}$$

where Z is the cell impedance and, I_{ref} is the current. The voltage is linearly related to the output current,

$$I_{out} \approx Scale.\ (V_+ - V_-) \tag{10}$$

Therefore, the cell membrane impedance is,

$$Z(i) = \frac{I_{out\,(i)}}{Scale.\ I_{ref\,(i)}} \tag{11}$$

where scale is implemented as a current, through a current multiplier and is used for encompassing the scale factor (Hamilton et al., 2009).

In principle, impedance spectroscopy can also be implemented in the time domain, which is advantageous since speed will improve (Spencer et al., 2017). A bridge measurement system followed by signal conditioning may be used. An overall comparison of CMOS designs to measure impedance is illustrated in Table 2. The speed of the circuit in time and frequency domain designs is proportional to the clock of the circuit, and is related to the time delay. In the first group, the switches and blocks are used to convert and digitalize the measured time, therefore, the size is bigger in comparison to the other techniques. For lock-in amplifiers, a more complicated calculation is needed to extract the imaginary and real portions. For the impedance to frequency converter, the R and C value is measured in comparison to a known value, making the calculation relatively effortless.

To better discuss and compare different topologies, a figure of merit was devised as shown in Table 2. For all parameters, a smaller number would lead to a more compact, less power consuming design. As seen, the figure of merit for printed circuit board (PCB) designs is, as expected, far from integrated designs. Among the fabricated integrated designs, type 2 architectures are more advantageous in terms of compactness and low power. Table 2 gives an in depth comparison of recent publications on CMOS designs for impedance measurement.

In recent years, with advancement in fabrication technology and circuits designed with lower power consumption, many arrays or multifunction systems for cell impedance sensing have been proposed. An array of more than 50,000 microelectrodes have been proposed in order to measure cell impedance and record electrophysiological signals on the same chip. Using this array, position, adhesion, and the electrical activity of cardiac embryoid bodies can be measured and monitored (Viswam et al., 2016, 2018). In another approach, multi–modality arrays have been proposed (Chi et al., 2015; Park et al., 2017). These arrays combine cellular voltage recording, impedance measurement (voltage excitation/current sensing), and optical detection along with other sensors, i.e., temperature sensor, to provide comprehensive biological data in cell-based assay and drug screening applications. Integrating multiple sensors will increase the power and area, increasing design challenges and system complexity. This can lead to having a single readout circuit for each group of sensors that would force the system to have multiplexers, decoders, and even memory units. The result is that the system may be slower, necessitating design strategies to maintain high-speed high throughput measurements.

5.4. Capacitive sensors

In sections 5.1-5.3, all the readout systems measure the complex impedance of the cells. However, for some applications, measuring only the capacitance may be sufficient. Measuring capacitance is easier than measuring complex impedance, in the sense that in impedance sensing both capacitive and resistive part of a substance is measured. Capacitive sensing circuits have smaller circuits and don't need both imaginary and real part of the signal to do the calculation and offer the opportunity for new techniques. Several techniques have been used to measure cell capacitance, including charge based capacitance measurement (CBCM), charge share, and capacitance to frequency.

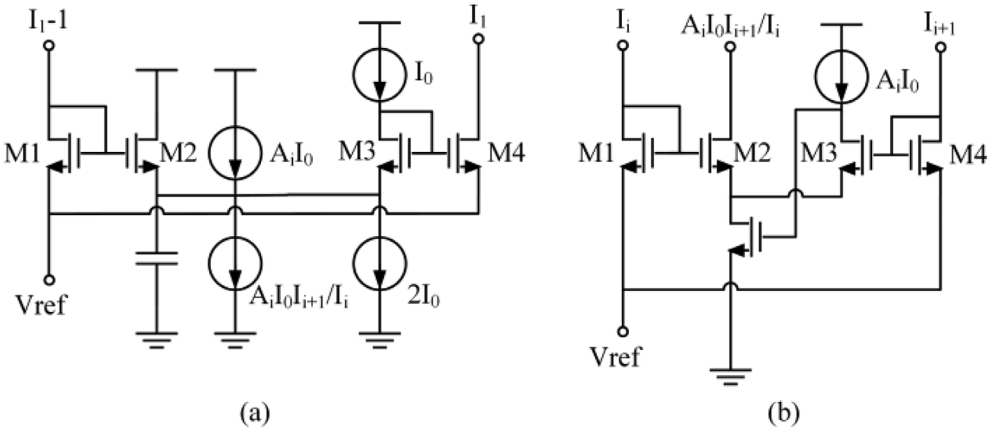

Fig. 11. Basic structure (a) and the feedback circuit (b) of the Tau-cell (Gu, 2016).

Table 2
CMOS impedance sensing comparison.

	Type[a]	Accuracy	# of Electrode	Technology (μm)	Area (mm^2)	Frequency range	Power (μW)	F.O.M[b]
Gu and McFarlane, 2012	2	Magnitude deviation < 7% Phase deviation < 4%.	1	0.13	~0.01	100 Hz, 1 kHz, 10 kHz, 100 kHz	207.2	0.02
Mucha, 2012	1	Cell adhesion and death detected reliably, ~10%	64	0.35	~2	Min. 1 kHz Max. 50 kHz	~200	0.22
Vooka and George, 2015	2	0.04%(mode R) 0.15% (mode C)	1	PCB	500	Designed for 1 kHz	175.8×10^3	36×10^3
Liu, 2009	2	mismatch of 1%	1	0.5	0.045	Min. 0.01 kHz Max. 10 kHz	5.2	0.001
Hsu et al., 2018	1	0.04% Phase	1	0.18	0.02	Min. 5 kHz Max. 1 MHz	197	0.0003
Manickam et al., 2010	2	~1.4%	100	0.35	1	Min. 10 Hz Max. 50 MHz	84.8×10^3	4.24
Jafari et al., 2012	2	1% error	16	0.13	1.68	Min. 1 kHz Max. 10 kHz	350	0.05
Yang, 2008	1	RMS error of 0.027	1	0.5	0.06	Min. 100 Hz Max. 1 MHz	6	0.005
Ali, 2015	1.	0.41% (mode R) 0.73% (mode C)	12	0.18	2.7	Min. 1 Hz Max. 10 MHz	87	0.015
Kassanos et al., 2013	2	1.78° ± 0.115° Phase @50k 98% ± 0.6% Mag @50K	1	0.35	0.4	Min. 100 Hz Max. 100 kHz	21×10^3	17.64
Rottigni et al., 2011	2	~20%	1	0.35	0.9	up to 5 MHz	USB-powered	630
Yufera and Rueda, 2009	2	accuracy of ± 0.05	64	0.35	~1	Min. 10 kHz Max. 100 kHz	~100	0.02
Dungan et al., 2014	2	0.05% variation	1	0.13	~1	Max. 100 KHz	~100	0.006
Chen et al., 2017	2	0.12% Phase 0.28% Mag	1	0.35	0.07	Min. 0.1 Hz Max. 100 kHz	150	0.004
Rodriguez et al., 2016	2	1% error	2	0.15	1.5	Min. 2 kHz Max. 2 MHz	165	0.185
Allegri et al., 2018	2	0.8%	2	0.35	19.38	Min. 10 kHz Max. 10 MHz	100×10^3	2×10^3
Viswam et al., 2018	2	0.5% Phase	1	0.18	0.1	Min. 1 Hz Max. 1 MHz	412	0.03
Hamilton et al., 2009	3	average measurement error 2%	100	0.5	4	Min. 25 Hz Max. 100 MHz	30	0.012

[a] Type 1 = impedance to time/frequency domain, Type 2 = Lock-in amplifier with frequency sweep Type 3 = lock-in amplifier in wideband.
[b] Figure of merit was devised to have an overall parameter to compare the performance of designed circuit. For all the parameters we noticed that smaller number will lead to a more compact, less power consuming design. We defined figure of merit as below, so that the smaller FOM will show a better design.

$$FOM = \frac{accuracy \times area\ (mm^2) \times technology\ (\mu m) \times power\ (\mu W)}{\#\ of\ electrode}$$

Charge based capacitance measurements method were proposed to measure the cross-talk capacitance between the conductors in CMOS chips with the use of an off-chip DC ammeter (Sylvester et al., 1998). More recent implementations also used this technique for lab-on-a-chip purposes (Ghafar-Zadeh et al., 2007). In CBCM, the difference between the current that goes through the reference and sensing electrode is measured, and the difference is changed to voltage. Thus an increase or decrease of the sensing electrode can be measured in comparison to the reference electrode.

Fig. 12 is an example for CBCM circuit where the difference between two charging currents I_S and I_R is proportional to ΔC. When applying two non-overlapping clocks, Φ1 and Φ2, transduce the measured capacitances (C_S and C_R) into two currents. The current mirrors senses and amplifies these currents. Subtraction of these currents, ΔI, is performed through M9-M13, and ΔI is integrated and converted to voltage by C_{int}. The voltage drop at the output is, therefore, proportional to change of capacitance sensed in comparison to the reference capacitance. In (Nabovati et al., 2017, 2018) new developments for this method including a fully differential chip, no post processing, low power, and continuous measurement have reduced power consumption and cost significantly per biological experiment.

Parkash et al. presented an adaptation of charge based sharing for cell capacitance measurement (Prakash et al., 2005). The sensor circuit in this method, shown in Fig. 13, had two nodes with parasitic capacitances which are charged and discharged. With an increase in capacitance, the voltage on the joint electrode increases. Minimization of the parasitic capacitances maximize sensitivity and increase in the area of the metal electrode increases the dynamic range (Prakash et al., 2005).

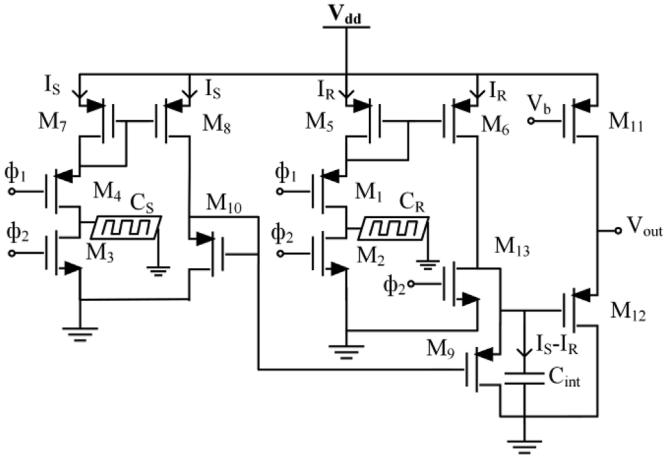

Fig. 12. Core-CBCM capacitive sensor circuit topology (Nabovati et al., 2017).

In many implementations, the topmost metal layer in the fabrication

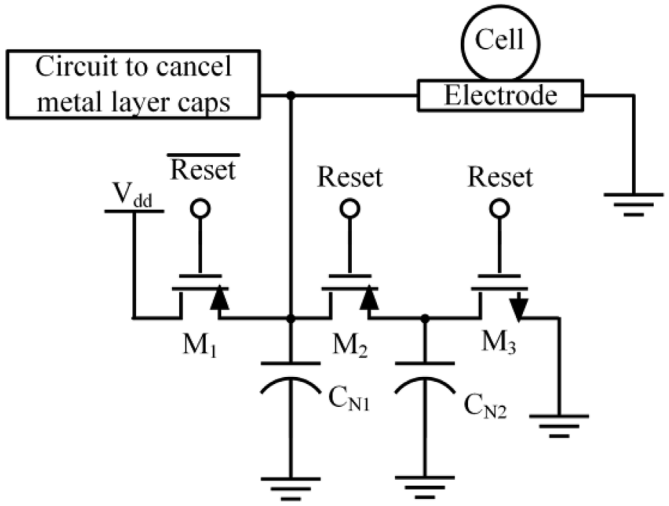

Fig. 13. Cell-substrate capacitance sensor measurement in charge sharing method (Prakash et al., 2005).

process forms the sensing electrode. And the layer below it acts as a shield for the sensing circuit. This method has been used to measure the capacitance of whole-cell bacteria(Couniot et al., 2016). The method has also been used with frequency readout (Mohammad et al., 2016; Senevirathna et al., 2017, 2018). Unlike other impedance measurement methods, capacitance to frequency designs does not require complex readout systems and is easily digitized.

6. Discussion

Integrated biosensors have been effective in whole cell based impedance sensing for various applications. The circuit topologies for cell impedance measurement were divided into 1. impedance to frequency conversion, 2. swept frequency, and 3. simultaneous frequencies topologies. There are many challenges and areas for improvement including the electrodes, spatial resolution, and highly parallel experimentation (high throughput with high speed). Impedance measurements have been typically performed using expensive and bulky benchtop instruments (An et al., 2019; Bagnaninchi and Drummond, 2011; Bird and Kirstein, 2009; Cho and Thielecke, 2008; Cui et al., 2017; Keese et al., 2004; Mamouni and Yang, 2011; McCoy and Wang, 2005).

Benchtop systems only have one or at most two inputs. This places an upper limit on the number of electrodes that can be measured at once and limits the readout time. To improve this limitation, adding on-chip signal processing units, such as the magnitude and phase calculation analog circuits, can lower area and power consumption. The power consumption of integrated designs are on average ~100 μW, for discrete systems, this number is in the range of 100 mW, which is 100 times more than an integrated readout system. In terms of area, the integrated systems average 0.1 mm^2, while a typical discrete PCB for impedance measurement can have areas of 500 mm^2 (Vooka and George, 2015), thus integrating readout electronics can lead to up to a 99% reduction in area consumption.

These systems need to sweep frequencies, which also places a limit on the readout time. The CMOS implementation has the potential of facilitating the fabrication while having a low cost. Based on a recent commercially available process (28nmlithographyprocess), a standard die size is between 100 mm^2 to 300 mm^2. Taking an average of 0.1 mm^2 for a readout system per channel will give over 1000 to 3000 chips per run, having a cost of readout system at ~$3 for a unit research chip and less for a commercial chip. For a typical discrete and benchtop readout system, this price will be in range of $100. With 3-D printing advancement, highly sensitive and compact CMOS bio-sensors are believed to be the next generation of lab-on-a-chip and micro-total analysis platforms. Moreover, 3-D printed electrodes can lead the way in introducing cheap and disposable electrodes to grow cells and measure their characteristics (Zia et al., 2015, 2016).

Table 2 shows a comparison among proposed CMOS cell impedance measurement topologies. While all realize a low form factor, they do not all address parallel/multiple measurements or decreasing the measurement time window. Additionally, many of these implementations do not take advantage of the inherent parallelism offered by the technology. Implementation in CMOS allows for the reduced cost due to the maturity of the process and a higher degree of parallelism due to a more integrated system incorporating signal processing and analog to digital conversion. Additionally, it allows for the system to have a small form factor and low power requirements. Currently, impedance is not a specific measurement, and other measurements must be made for interpretation. This includes temperature measurements and observing visually (optical measurements).

Commercially available electrodes for impedance spectroscopy are in the range of 100–300 μm, while cells tend to be less than 100 μm, and many interesting ones are around 10 μm. Therefore, the spatial resolution of the system improves as the system, particularly the electrodes, gets smaller (Xu et al., 2016). For improving the system, more than one electrode can be in contact with a single cell. However, this is different from current fabrication techniques, particularly the commercial techniques. Size limitations on planar electrodes is approximately 10 μm in size with a 10 μm pitch (Giaever and Keese, 2012). Other micro and nanofabrication techniques have been used to develop sub-micrometer electrodes. These include the use of carbon nanofibers, which make the electrode sizes in the range of 10–100 nm and reduces the size by the factor of 10^3 (Galos and Li, 2016; Yu et al., 2015). The carbon nanotube towers can be easily peeled off a silicon substrate and soldered onto printed circuit board.

~ Shows the values are estimated or assumed since was not mentioned in the reference.

Regarding sensitivity, the topologies are divided into three groups. In the first group, (Liu et al., 2009; Mucha, 2012), the comparator design is the main block for the impedance measurement block, changing the voltage to frequency. In this group, the sensitivity is limited by the current passing through the amplification stage of the comparator (I). This current is proportional to the input voltage difference (ΔV_{in}), tail transistor size (K) (the transistor that biases the amplification stage), and the current that is passing through it.

$$Sensitivity \propto \Delta V_{in} \times K \times I \tag{12}$$

In the second group, (Kassanos et al., 2013; Manickam et al., 2010; Vooka and George, 2015; Yufera and Rueda, 2009), a current amplifier amplifies the small current passing through the cell to a bigger voltage or current. Therefore, in addition to the accuracy of the technology to fabricate matching transistors, the dynamic range (DR) of the amplifier has a huge role in sensitivity,

$$Sensitivity \propto DR \times K \times I \tag{13}$$

In the third group, (Gu, 2016; Hamilton et al., 2009), the design consists of filters and current biases. The primary limiting issue to have a more sensitive system is the fabrication technology's ability to fabricate matching transistors. Thus, the sensitivity is proportional to σI_{ref}, the smallest difference in reference current achievable.

$$Sensitivity \propto \sigma_{I_{ref}} \times K \times I \tag{14}$$

As fabrication technology advances and challenges for more compact fabrication are overcome, multiple methods can be combined for an analyzing system. As an example, a hydrogel-based cell chip was combined with impedance spectroscopy for improved drug screening. Hydrogel tissue mimicking structure can be implemented using microfluidic channels (Tran et al., 2013). Other future applications include the development of low-cost devices for specific functions. Trans-

well migration assays quantify the motility of endothelial cells in blood vessel formation. Implementation of impedance spectroscopy for trans-well assays have been commercialized for epithelial ovarian carcinoma (EOC) and in Bird and Kirstein to detect cancerous varying migratory and invasive behaviors. ECIS can substitute for traditional trans-well assays (Bifulco et al., 2014), (Bird and Kirstein, 2009). Another challenge in cell impedance sensing is signal variation. The detected fluctuation in signals can be μA or μV range. Measurement using multiple electrode arrays offers measurement repetition. Various fitting methodologies can also be applied. Implementing mathematical functions using standard digital processing techniques can be bulky and power consuming, implying that analog and integrated solutions may be more appropriate.

7. Conclusion

In summary, there are still many challenges before these whole cell CMOS based impedance systems can replace state of the art chemical and optical methods. These challenges include overall packaging of the system, the electrodes, and the electronics used for readout and signal processing. Future designs can have a miniaturized readout system, thus making it possible to have a readout system for every single electrode. Eliminating the need for multiplexers and counters can contribute to reduced cost and power consumption. Digitizing blocks and signal processing along with multiarray electrode systems will make a complete biological impedance sensor at the microscale. A whole system that can sense cellular anomalies, process sensed data, and store or transmit wirelessly can be implanted for health monitoring. Implanted cell monitoring systems can report cell changes when it happens leading to a new generation of sensors. To make this possible, electronic circuits need to be smaller and flexible. Further advancements can utilize circuits etched in biomaterials (eg. DNA) instead of silicon.

These challenges are solvable and will rely heavily on solutions used in other fields. The advancements needed to improve this technology can also lie in the proliferation of nano sized devices for size reduction. The prospective future of this technology is for a multi sensing system that can measure different biological characteristics and the cell environment such as acidity, temperature, impedance, and potential all on a single chip. The measuring system can share the readout system, thus saving on power and area. Power is another challenge regarding these sensors. Even μW power consumption, if arrayed to many electrodes, can be problematic. Power consumption of circuits increases the temperature in cells and tissues. Temperature increases as small as 1 °C can kill sensitive cells. This again leads to the requirement of lower operating voltages which in turn leads to decreasing the size to nm or less range. Despite these challenges, CMOS based biological cell impedance sensing, particularly if combined with other sensors, offers the potential for achieving low power, multi-function, real-time diagnosis for many applications which will impact scientific discovery and disease diagnosis.

CRediT authorship contribution statement

Ava Hedayatipour: Conceptualization, Investigation, Resources, Writing - original draft, Writing - review & editing, Visualization, Project administration. **Shaghayegh Aslanzadeh:** Investigation, Resources, Writing - original draft, Writing - review & editing, Visualization. **Nicole McFarlane:** Conceptualization, Investigation, Writing - review & editing, Supervision.

Declaration of competing interest

The authors declare that they have no known competing financial interests or personal relationships that could have appeared to influence the work reported in this paper.

Acknowledgement

This research did not receive any specific grant from funding agencies in the public, commercial, or not-for-profit sectors.

Patient consent: Consent to publish the case report was not obtained. This report does not contain any personal information that could lead to the identification of the patient. Funding: No funding or grant support. Authorship: All authors attest that they meet the current ICMJE criteria for Authorship. Conflict of interest: The following authors have no financial disclosures: (Authors initials).

References

28nmlithographyprocess https://www.samsung.com/semiconductor/insights/news-events/samsung-qualifies-28nm-lp-process-technology-for-high-performance-mobile-applications/ (Accessed 03/2019.).
Abiri, H., Abdolahad, M., Gharooni, M., Hosseini, S.A., Janmaleki, M., Azimi, S., Hosseini, M., Mohajerzadeh, S., 2015. Biosens. Bioelectron. 68, 577–585.
ACEA Biosciences Inc, xCELLigence System https://www.aceabio.com/products/xcelligence-rtca/ (Accessed Accessed 03/2019.).
Adiguzel, Y., Kulah, H., 2012. Sensors 12 (8), 10042–10066.
Albrecht-Buehler, G., 1977. Cell 11 (2), 395–404.
Ali, A., Pal, N., Levine, P.M., 2015. EEE Int. Midwest Symp. Circuits Syst.. 1–4.
Allegri, D., Donida, A., Malcovati, P., Barrettino, D., 2018. IEEE Trans. Biomed. Circuits Syst. 12 (6), 1301–1312.
An, Yu, Jin, Tongyu, Zhang, Fan, He, Pingang, 2019. Electric cell-substrate impedance sensing (ECIS) for profiling cytotoxicity of cigarette smoke. Journal of Electroanalytical Chemistry 834, 180–186.
Anh-Nguyen, T., Tiberius, B., Pliquett, U., Urban, G.A., 2016. Sens. Actuators A Phys. 241, 231–237.
Applied BioPhysics Inc ECIS TEER 24. http://www.biophysics.com/products-ecisTeer24.php Accessed 03/2019.
Applied BioPhysics Inc ECIS Zθ (Theta). http://www.biophysics.com/products-ecisz0.php Accessed 03/2019.
Bagnaninchi, P.O., Drummond, N., 2011. Proc. Natl. Acad. Sci. 108 (16), 6462–6467.
Bifulco, K., Votta, G., Ingangi, V., Di Carluccio, G., Rea, D., Losito, S., Montuori, N., Ragno, P., Stoppelli, M.P., Arra, C., 2014. Oncotarget 5 (12), 4154.
Bird, C., Kirstein, S., 2009. Nat. Methods 6 (8).
Bondu, V., Schrader, R., Gawinowicz, M.A., McGuire, P., Lawrence, D.A., Hjelle, B., Buranda, T., 2015. Viruses 7 (2), 559–589.
Bordi, F., Cametti, C., Gili, T., 2002. J. Non-Cryst. Solids 305 (1–3), 278–284.
Caselli, F., Bisegna, P., Maceri, F., 2010. J. Microelectromech. Syst. 19 (5), 1029–1040.
Caselli, F., De Ninno, A., Reale, R., Businaro, L., Bisegna, P., 2018. Sens. Actuators B Chem. 256, 580–589.
Chen, T.-A., Wu, W.-J., Wei, C.-L., Darling, R.B., Liu, B.-D., 2017. IEEE Trans. Biomed. Circuits Syst. 11 (2), 370–379.
Chi, T., Park, J.S., Butts, J.C., Hookway, T.A., Su, A., Zhu, C., Styczynski, M.P., McDevitt, T.C., Wang, H., 2015. IEEE Trans. Biomed. Circuits Syst. 9 (6), 801–814.
Cho, S., Thielecke, H., 2008. Microelectron. Eng. 85 (5), 1272–1274.
Cho, S., Gorjup, E., Thielecke, H., 2009. Annals of Anatomy-Anatomischer Anzeiger 191 (1), 145–152.
Corcoran, C., Rechnitz, G., 1985. Trends Biotechnol. 3 (4), 92–96.
Couniot, N., Francis, L.A., Flandre, D., 2016. IEEE Trans. Biomed. Circuits Syst. 10 (2), 364–374.
Cui, Y., An, Y., Jin, T., Zhang, F., He, P., 2017. Sens. Actuators B Chem. 250, 461–468.
Dandin, M., Jung, I.D., Piyasena, M., Gallagher, J., Nelson, N., Urdaneta, M., Artis, C., Abshire, P., Smela, E., 2009. IEEE Sensors Conference 795–798.
Davey, H.M., Kell, D.B., 1996. Microbiol. Rev. 60 (4), 641–696.
De Ninno, A., Errico, V., Bertani, F.R., Businaro, L., Bisegna, P., Caselli, F., 2017. Lab Chip 17 (6), 1158–1166.
Dungan, J., Mathews, J., Levin, M., Koomson, V., 2014. In: IEEE 60th International Midwest symposium on Circuits and Systems (MWSCAS), pp. 56–59.
Edmondson, R., Broglie, J.J., Adcock, A.F., Yang, L., 2014. Assay Drug Dev. Technol. 12 (4), 207–218.
Ehret, R., Baumann, W., Brischwein, M., Schwinde, A., Wolf, B., 1998. Med. Biol. Eng. Comput. 36 (3), 365–370.
Errico, V., De Ninno, A., Bertani, F.R., Businaro, L., Bisegna, P., Caselli, F., 2017. Sens. Actuators B Chem. 247, 580–586.
Esfandyarpour, R., DiDonato, M.J., Yang, Y., Durmus, N.G., Harris, J.S., Davis, R.W., 2017. Proc. Natl. Acad. Sci 201621318.
Evander, M., Ricco, A.J., Morser, J., Kovacs, G.T., Leung, L.L., Giovangrandi, L., 2013. Lab Chip 13 (4), 722–729.
Foster, K.R., Sauer, F.A., Schwan, H.P., 1992. Biophys. J. 63 (1), 180–190.
Fu, T.-M., Hong, G., Viveros, R.D., Zhou, T., Lieber, C.M., 2017a. Proc. Natl. Acad. Sci. 114 (47), E10046–E10055.
Fu, Y., Yuan, Q., Guo, J., 2017b. Microfluid. Nanofluidics 21 (2), 20.
Galos, Richard, Li, Xin, 2016. Electrical Impedance Measurements of PZT Nanofiber Sensors. In: Proceedings of the ASME 2016 International Design Engineering Technical Conferences and Computers and Information in Engineering Conference. Volume 4: 21st Design for Manufacturing and the Life Cycle Conference; 10th International Conference on Micro- and Nanosystems. August 21–24.
Gawad, S., Schild, L., Renaud, P., 2001. Lab Chip 1 (1), 76–82.

Ghafar-Zadeh, E., Sawan, M., Therriault, D., 2007. Sens. Actuators A Phys. 134 (1), 27–36.
Giaever, I., Keese, C.R., 1984. Proc. Natl. Acad. Sci. 81 (12), 3761–3764.
Giaever, I., Keese, C.R., 1986. IEEE Trans. Biomed. Eng. (2), 242–247.
Giaever, I., Keese, C.R., 1991. Proc. Natl. Acad. Sci. 88 (17), 7896–7900.
Giaever, I., Keese, C.R., 1993. Nature 366 (6455), 591–592.
Giaever, I., Keese, C.R., 2012. Electric Cell-Substrate Impedance Sensing Concept to Commercialization, Electric Cell-Substrate Impedance Sensing and Cancer Metastasis. Springer, pp. 1–19.
Goda, N., Kataoka, N., Yamamoto, Y., Okuda, H., Kajiya, F., 2004. IEEE Int. Midwest Symp. Circuits Syst iii-223.
Gu, J., 2016. Electrical Engineering. University of Tennessee, Knoxville.
Gu, J., McFarlane, N., 2012. EEE Int. Midwest Symp. Circuits Syst. 1016–1019.
Gu, J., McFarlane, N., 2015. In: IEEE Instrumentation and Measurement Technology Conference ,, pp. 494–499.
Hamilton, T.J., Nelson, N.M., Sander, D., Abshire, P., 2009. In: IEEE Biomedical Circuits and Systems Conference, pp. 117–120.
Han, A., Yang, L., Frazier, A.B., 2007. Clin. Cancer Res. 13 (1), 139–143.
Hildebrandt, C., Büth, H., Cho, S., Thielecke, H., 2010. J. Biotechnol. 148 (1), 83–90.
Holmes, D., Pettigrew, D., Reccius, C.H., Gwyer, J.D., van Berkel, C., Holloway, J., Davies, D.E., Morgan, H., 2009. Lab Chip 9 (20), 2881–2889.
Hsu, C.-L., Sun, A., Zhao, Y., Aronoff-Spencer, E., Hall, D.A., 2018. In: IEEE Custom Integrated Circuits Conference, pp. 1–4.
Itano, N., Okamoto, S.-i., Zhang, D., Lipton, S.A., Ruoslahti, E., 2003. Proc. Natl. Acad. Sci. 100 (9), 5181–5186.
Jafari, H., Soleymani, L., Genov, R., 2012. IEEE Trans. Biomed. Circuits Syst. 6 (5), 468–478.
Jang, L.-S., Wang, M.-H., 2007. Biomed. Microdevices 9 (5), 737–743.
Kassanos, P., Triantis, I.F., Demosthenous, A., 2013. IEEE Sens. J. 13 (6), 2229–2236.
Keese, C.R., Wegener, J., Walker, S.R., Giaever, I., 2004. Proc. Natl. Acad. Sci. U. S. A 101 (6), 1554–1559.
Kilani, M.M., Mohammed, K.A., Nasreen, N., Hardwick, J.A., Kaplan, M.H., Tepper, R.S., Antony, V.B., 2004. CHEST J. 126 (1), 186–191.
Kim, T., Han, G., Han, M., 2017. In: IEEE International Midwest Symposium on Circuits and Systems. MWSCAS), pp. 1621–1624.
Koledintseva, M.Y., DuBroff, R.E., Schwartz, R.W., 2006. Missouri University .
Krishna, R., Paschek, D., 2000. Separ. Purif. Technol. 21 (1–2), 111–136.
Kweon, S.-J., ParN, J.-H., Shin, S., Yoo, S.-S., Yoo, H.-J., 2017. In: IEEE International Midwest Symposium on Circuits and Systems, pp. 1037–1040.
Lauffenburger, D.A., Horwitz, A.F., 1996. Cell 84 (3), 359–369.
Lei, K.-M., Mak, P.-I., Law, M.-K., Martins, R.P., 2016. Lab Chip 16 (19), 3664–3681.
Levsky, J.M., Singer, R.H., 2003. Trends Cell Biol. 13 (1), 4–6.
Li, H., Liu, X., Li, L., Mu, X., Genov, R., Mason, A., 2017. Sensors 17 (1), 74.
Liao, C.-S., Lee, G.-B., Liu, H.-S., Hsieh, T.-M., Luo, C.-H., 2005. Nucleic Acids Res. 33 (18) e156-e156.
Liu, X., Rairigh, D., Yang, C., Mason, A.J., 2009. IEEE Int. Symp. Circuits Syst. 353–356.
Luo, T., Li, L., Ghorband, V., Zhan, Y., Song, H., Christen, J.B., 2016. In: IEEE International Symposium on Circuits and Systems, pp. 2891–2894.
Luong, J.H., Habibi-Rezaei, M., Meghrous, J., Xiao, C., Male, K.B., Kamen, A., 2001. Anal. Chem. 73 (8), 1844–1848.
Mamouni, J., Yang, L., 2011. Biomed. Microdevices 13 (6), 1075–1088.
Manickam, A., Chevalier, A., McDermott, M., Ellington, A.D., Hassibi, A., 2010. IEEE Trans. Biomed. Circuits Syst. 4 (6), 379–390.
McCoy, M.H., Wang, E., 2005. J. Virol Methods 130 (1), 157–161.
McGuinness, R., 2007. Curr. Opin. Pharmacol. 7 (5), 535–540.
Micronit Microtechnologies Inc Electrical impedance spectroscopy. https://www.micronit.com/products/electrical-impedance-spectroscopy.html Accessed 03/2019.
Mohammad, K., Buchanan, D.A., Thomson, D.J., 2016. In: IEEE Biomedical Circuits and Cystems Conference ,, pp. 22–25.
Mohanty, S.K., Ravula, S.K., Engisch, K.L., Frazier, A.B., 2003. Int. Conf. on Solid-State Sens., Actuators Microsyst. 1055–1058.
Morgan, H., Sun, T., Holmes, D., Gawad, S., Green, N.G., 2006. J. Phys. D Appl. Phys. 40 (1), 61.
Mucha, A., 2012. Universität München.
Mussa-Ivaldi, F.A., Miller, L.E., 2003. Trends Neurosci. 26 (6), 329–334.
Nabovati, G., Ghafar-Zadeh, E., Letourneau, A., Sawan, M., 2017. IEEE Trans. Biomed. Circuits Syst. 11 (2), 380–391.
Nabovati, G., Ghafar-Zadeh, E., Letourneau, A., Sawan, M., 2018. IEEE Trans. Biomed. Eng.
Narayanamurthy, V., Nagarajan, S., Samsuri, F., Sridhar, T., 2017. Analytical Methods.
Nguyen, T.A., Yin, T.-I., Urban, G., 2013. IEEE Sensors Conference. pp. 1–4.
Nicolelis, M.A., 2003. Nat. Rev. Neurosci. 4 (5), 417.
Nolan, J.P., Sklar, L.A., 2002. Trends Biotechnol. 20 (1), 9–12.
Nordberg, R.C., Zhang, J., Griffith, E.H., Frank, M.W., Starly, B., Loboa, E.G., 2017. Stem Cells Transl. Med. 6 (2), 502–511.
NuVant Systems Inc Ezware. http://nuvant.com/download-software/software/ Accessed 03/2019.
Parak, W., Domke, J., George, M., Kardinal, A., Radmacher, M., Gaub, H., De Roos, A., Theuvenet, A., Wiegand, G., Sackmann, E., 1999. Biophys. J. 76 (3), 1659–1667.
Park, J., Aziz, M.K., Gonzalez, S., Jung, D., Chi, T., Li, S., Cho, H.C., Wang, H., 2017. In: IEEE Custom Integrated Circuits Conference, 2017, pp. 1–4.
Park, C.-Y., Min, J.-H., Kim, Y.-S., Song, H.-J., Kim, J.-D., 2019. Sens. Mater. 31 (2), 253–259.
Pavlin, M., Miklavčič, D., 2003. Biophys. J. 85 (2), 719–729.
Pennington, M.R., Van de Walle, G.R., 2017. mSphere 2 (2) e00039-00017.
Prakash, S.B., Abshire, P., Urdaneta, M., Smela, E., 2005. In: . IEEE International Cymposium on Circuits and Systems. pp. 3495–3498.
Racek, J., 1995. Cell-based biosensors. CRC Press.
Reddy, L., Wang, H.-S., Keese, C.R., Giaever, I., Smith, T.J., 1998. Exp. Cell Res. 245 (2), 360–367.
Reitinger, S., Wissenwasser, J., Kapferer, W., Heer, R., Lepperdinger, G., 2012. Biosens. Bioelectron. 34 (1), 63–69.
Rodriguez, S., Ollmar, S., Waqar, M., Rusu, A., 2016. IEEE Trans. Biomed. Circuits Syst. 10 (3), 533–544.
Rottigni, A., Carminati, M., Ferrari, G., Sampietro, M., 2011. 7th Conf. on Ph. D. Research in Microelectronics and Electronics. IEEE, pp. 49–52.
Senevirathna, B., Lu, S., Abshire, P., 2017. In: IEEE International Symposium on Circuits and Systems, pp. 1–4.
Senevirathna, B.P., Lu, S., Dandin, M.P., Basile, J., Smela, E., Abshire, P.A., 2018. IEEE Trans. Biomed. Circuits Syst.
Sengupta, S., Lohse, C.M., Leibovich, B.C., Frank, I., Thompson, R.H., Webster, W.S., Zincke, H., Blute, M.L., Cheville, J.C., Kwon, E.D., 2005. Cancer 104 (3), 511–520.
Shah, P., Zhu, X., Zhang, X., He, J., Li, C.-z., 2016. ACS Appl. Mater. Interfaces 8 (9), 5804–5812.
Solly, K., Wang, X., Xu, X., Strulovici, B., Zheng, W., 2004. Assay Drug Dev. Technol. 2 (4), 363–372.
Spencer, Edmund, David, Clark, Ravi, Gollapalli, Samuel, Russ, Brannon, Kerrigan, 2017. A System On Chip design for fast time domain impedance spectroscopy. In: 2017 IEEE 60th International Midwest Symposium on Circuits and Systems (MWSCAS). IEEE, pp. 124–127.
Sun, T., Morgan, H., 2010. Microfluid. Nanofluidics 8 (4), 423–443.
Sun, T., Gawad, S., Green, N.G., Morgan, H., 2006. J. Phys. D Appl. Phys. 40 (1), 1.
Sun, T., Tsuda, S., Zauner, K.-P., Morgan, H., 2009. Nano/Micro Engineered and Molecular Systems, 2009. NEMS 2009. 4th IEEE International Conference on. IEEE, pp. 858–863.
Sylvester, D., Chen, J.C., Hu, C., 1998. IEEE J. Solid State Circuits 33 (3), 449–453.
Talukder, N., Furniturewalla, A., Le, T., Chan, M., Hirday, S., Cao, X., Xie, P., Lin, Z., Gholizadeh, A., Orbine, S., 2017. Biomed. Microdevices 19 (2), 36.
Tran, T.B., Cho, S., Min, J., 2013. Biosens. Bioelectron. 50, 453–459.
Tran, T.B., Baek, C., Min, J., 2016. PLoS One 11 (4), e0153813.
Viswam, V., Raziyeh, B., Amir, S., Jelena, D., Alicia, B.J., Axel, B., Jan, M., Yihui, C., Andreas, H., 2016. IEEE Sensors. pp. 1–3.
Viswam, V., Bounik, R., Shadmani, A., Dragas, J., Urwyler, C., Boos, J.A., Obien, M., Muller, J., Chen, Y., Hierlemann, A., 2018. IEEE Trans. Biomed. Circuits Syst. 1356–1368.
Vogler, E.A., 1988. Biophys. J. 53 (5), 759–769.
Vooka, P., George, B., 2015. IEEE Trans. Ind. Meas. 64 (4), 902–912.
Walker, G.M., Beebe, D.J., 2002. Lab Chip 2 (3), 131–134.
Wang, L., Zhu, J., Deng, C., Xing, W.-l., Cheng, J., 2008. Lab Chip 8 (6), 872–878.
Wang, M.-H., Kao, M.-F., Jang, L.-S., 2011. Rev. Sci. Instrum. 82 (6), 064302.
Watkins, N.N., Sridhar, S., Cheng, X., Chen, G.D., Toner, M., Rodriguez, W., Bashir, R., 2011. Lab Chip 11 (8), 1437–1447.
Wegener, J., Janshoff, A., Galla, H.-J., 1998. Eur. Biophys. J. 28 (1), 26–37.
Wegener, J., Keese, C.R., Giaever, I., 2000. Exp. Cell Res. 259 (1), 158–166.
Wiest, J., Stadthagen, T., Schmidhuber, M., Brischwein, M., Ressler, J., Raeder, U., Grothe, H., Melzer, A., Wolf, B., 2006. Anal. Lett. 39 (8), 1759–1771.
Won, J.Y., Kwon, S.I., Yoon, H.S., Ko, G.B., Son, J.-W., Lee, J.S., 2016. IEEE Trans. Biomed. Circuits Syst. 10 (1), 231–242.
Xavier, M., de Andrés, M.C., Spencer, D., Oreffo, R.O., Morgan, H., 2017. J. R. Soc. Interface 14 (133), 20170233.
Xiao, C., Luong, J.H., 2003. Biotechnol. Prog. 19 (3), 1000–1005.
Xu, Y., Xie, X., Duan, Y., Wang, L., Cheng, Z., Cheng, J., 2016. Biosens. Bioelectron. 77, 824–836.
Yang, C., Mason, A.J., 2008. Sensors. pp. 642–645.
Yang, J.-M., Chen, S.-W., Yang, J.-H., Wang, J.-S., 2011. Int. Conf. Biomed. Eng. Inf. 938–941.
Yang, Y., Jia, J., Smith, S., Jamil, N., Gamal, W., Bagnaninchi, P.-O., 2017. IEEE Sens. J. 17 (2), 514–523.
Yu, Y., Al Mamun, K.A., Islam, S.K., McFarlane, N., 2015. In: IEEE Nanotechnology Materials and Devices Conference, pp. 1–2.
Yufera, A., Rueda, A., 2009. Int. Symp. Design Diagn. Electron. Circuits Syst. 252–257.
Zhao, X., Zhuang, H., Yoon, S.-C., Dong, Y., Wang, W., Zhao, W., 2017. J. Food Qual.
Zia, M., Chi, T., Zhang, C., Thadesar, P., Hookway, T., Gonzalez, J., McDevitt, T., Wang, H., Bakir, M.S., 2015. In: IEEE Electron devices meeting. 29. pp. 24. 21–29.24. 24.
Zia, M., Chi, T., Park, J.S., Su, A., Gonzalez, J.L., Jo, P.K., Styczynski, M.P., Wang, H., Bakir, M.S., 2016. IEEE Trans. Compon. Packag. Manuf. Technol. 6 (12), 1827–1833.